# ELECTROCHEMICAL EVALUATION OF HUMIDITY BASED PROTON CONDUCTIVITY OF ALUMINIUM(III) TARTRATE

G.Bhuvaneswari[1], S.Rameshkumar1*

*[1] Department of Chemistry, Sri Vasavi College, Erode, India -638316.*

**Abstract:** Aluminium(III) tartrate was synthesized by simple solution crystallization and its humidity dependent proton conductivity was evaluated using electrochemical impedance spectroscopy. The compound exhibited very low DC conductivity and AC conductivity in the as synthesized form and dried conditions. However, upon exposing to 100% relative humidity(RH) the AC conductivity of the compound increased significantly with time and is several orders greater than DC conductivity. The structural stability of the compound was analysed by FTIR and PXRD experiments. The compound has good structural stability on hydration, dehydration and rehydration. The proton conductivity of the sample decreased several orders on dehydration and it bounces back to original value on rehydration. The complex exhibited reversible proton conductivity with respect to moisture. The variation of proton conductivity with temperature implies that the compound exhibits Grotthuss type proton conductivity.

Keywords: Coordination compounds; EIS; Relative humidity; Proton conductivity; Solution crystallization.

## 1. INTRODUCTION

The increased global energy consumption and the limitation of natural resources such as fossil fuels, the demand for energy by humans increases and estimated to double by 2050 [1,2]. Overutilization of non-renewable fossil fuels for the energy production produced large amount of carbon dioxide gas, which is major reason for global warming [3-5]. Development of renewable and eco-friendly energy solutions gained attracting widespread attention to move away from the non-renewable resources [6-8]. Even though certain renewable energy sources such as solar cells and wind mills replace the non-renewable resources with no environmental hazards, they are climate – dependent and less efficient [3]. Mild operating conditions, low to zero emission, energy conversion efficiency and extended durability made the fuel cells to be the best choice among the various advanced energy conversion and energy storage devices explored to throw away the problems faced in the non-renewable energy resources [9-12]. There are several types of fuel cells which are distinguished by the type of electrolyte used such as solid oxide, alkaline solution, metal carbonate, phosphoric acid and proton exchange membrane [13-16].

The proton exchange membrane fuel cells directly convert the chemical energy stored in a fuel into electrical energy [17]. The heart of the proton exchange membrane fuel cell is proton exchange membrane, which plays an important role in the proton transport. The commercially available proton exchange membranes are manufactured by a series of nafion series membranes consisting of polytetrafluoroethylene main chains and perfluoroethylene ether side chains of sulphonic acid groups [18,19]. However, when the temperature is higher than 80ºC the conductivity of these membranes starts to decrease pointedly and the preparation process of nafion membranes is complex [20]. Furthermore, the high cost of preparation and fuel crossover also limit their applications [21,22].

After the first demonstration of proton conductivity of coordination compounds [23], many research works have been carried out for the proton conductivity of coordination compounds. These coordination compounds are regarded as metal organic frameworks (MOFs), composed of metal ions or clusters inter connected by organic

linker molecules in extended three dimensional networks [24,25]. Recently some coordination compounds with specific pendants gained special attention for their proton conductivity [26]. However, many metal organic frame works and coordination compounds were not explored for their proton conductivity. The presence of charge carriers such as ammonium ions, protons, hydroxide ions or Lewis acid moieties with the hydrogen bonded network structure or arrays of water molecules in the three dimensional network structure give the impression for the proton conductivity to these complexes [27]. These metal organic frameworks, in addition have the advantages of pre synthesis design and post synthesis modification with porosity, a large internal surface area and tenability [28]. The tuneable frameworks, regular pores and controllable functional groups made the metal organic frameworks outstanding proton conductors. The structural features of the coordination compounds and metal organic frameworks suggested them to emerge as promising solid polymer electrolytes or membranes for various devices such as fuel cells [29], humidity sensors [30] and hydrogen sensors [31].

The present work is aimed to synthesize aluminium (III) tartrate complex by simple solution crystallization method and to evaluate the proton conductivity of the complex compound using electrochemical impedance spectroscopy at room temperature and high temperatures. The moisture dependent proton conductivity of the complex with time is described by evaluating electrochemical impedance parameters at different time interval. The structural changes on exposure to moisture is analysed by PXRD and FTIR methods. The proton conductivity of aluminium (III) tartrate at room temperature and high temperatures suggested that it can be a better candidate as proton exchange membrane at high temperatures and a moisture sensor.

## 2. Experimental

### 2.1 Materials

Tartaric acid crystals, aluminiumsulphate and sodiumcarbonate were purchased from Sigma Aldrich and used without further purification. Double distilled water was used for the preparation and dilution of all solutions. The synthesis and characterization of aluminium tartrate had been already reported in the literature [32], however its moisture dependent proton conductivity was not studied. Following the procedure using aluminium sulphate, sodium carbonate and L-tartaric acid, aluminium tartrate was synthesized.

### 2.2 FTIR Spectroscopy

The FTIR spectrum of the prepared complex was recorded using Shimadzu 8400S FTIR spectrometer. The FTIR spectrum was recorded as KBr pellet. The spectra were recorded for the sample prepared as such, after exposing to 100% RH for 24h and drying in desiccator.

### 2.3 X-ray powder diffraction

The PXRD experiments were performed on Shimadzu Lab Model 6000 Xrd instrument. The PXRD measurements were made for the freshly prepared compound, after exposing 100% RH and drying in a desiccator. The powdered sample was used for PXRD measurements.

### 2.4 Elemental analysis and molecular weight determination

The bulk purity of the sample was checked by elemental analysis of dried sample and the molecular mass was analysed freezing point depression using camphor. The C and H analyses were performed were performed on Thermofinnigan, Flash EA 1112 CHN as well as in the Elementar Vario ELIII analysers. The calculated values are C = 25.26% and H = 3.51% while the percentage of elements found C=24.79% and H=3.37%. The percentage of Al was calculated to be 9.47% and estimated in the lab to be 9.35%. The molecular weight of the compound was found to be 571.3 by cryoscopic method.

### 2.5 Structural optimization

Quantum chemical calculations were made for the optimization of geometry and to find out possible centres for hydrogen bonding. Geometry optimization was accomplished by Hartree-Fock level with the 3-21 G and 6-31 G(d,p) basis sets. The optimized geometry was used for calculating HOMO and LUMO of molecule and also to locate the possible hydrogen bonding interactions.

### 2.6 Proton conductivity of the sample

The crystals obtained from solution were powdered and pressed into pellets of diameter 1.3 cm and thickness 0.18 mm under a pressure of 100 $kgcm^{-2}$. The pellet was coated with silver paint on either sides and sandwiched between two conducting plates. The pellet is immobilized between the conducting plates on a homemade cell with a screw load. The sample was kept under 100% relative humidity and the electrochemical impedance spectra were recorded at different time intervals. The spectra were recorded by superimposing an sinusoidal voltage of amplitude 100 mV at the open circuit potential in the frequency range 1MHz to 10 mHz. The spectra were recorded using two probe method using Zahner Zennium XC potentiostat/Galvanostat instrument. The conductivity of the sample was calculated employing the expression,

$$\sigma = \frac{L}{z \times A}$$

Where, $\sigma, L, Z \text{ and } A$ respectively are conductivity (in $\Omega^{-1}$ $cm^{-1}$), thickness (in cm), impedance (in Ω) and area (in $cm^2$) of the sample.

The Nyquist plots obtained were analysed by fitting with suitable equivalent circuit. The electrochemical impedance parameters were obtained from the experimental results and the suitable equivalent circuits. Whenever required the sample was dried under a current of warm air at 60º C for 45 minutes.

## 3. 3.Results and Discussion

### 3.1 Synthesis and Structural analysis

The electrochemical impedance studies are in general made on the single or microcrystalline samples using compact pellets [33-37]. Such methods noticeably necessitate the availability of highly pure compounds in considerable quantities, which indicates the crucial role of synthetic conditions in the synthetic methods employed. Gel phase crystallization technique is a well-known route for the synthesis of metal tartrates [38-43], it seems an imperfect method for the present study because of likelihood of product contaminations by the incorporation of gel phase impurities in the crystals [44] which should be eliminated for the AC impedance studies. In addition, gel phase crystallization suffers by the long duration for crystallization which ranges from days to weeks for the crystallization. Hence, it is necessary to propose alternate method for the crystallization of aluminium tartrate for characterizing its conductivity by AC impedance studies.

In this connection, it is important to mention the significance of the present method of crystallization employed. This method involved simple mixing of relevant aqueous solutions of precursors under ordinary conditions at room temperature. The synthetic scheme is depicted in Fig.1. This route is based on our previous experience [27,45]. In this method L-tartaric acid and sodium carbonate solutions prepared separately are mixed in 1:1 mole ratio to produce sodium tartrate, the solution is warmed at 60º C for 30 minutes for the completion of the reaction. The solution is filtered in the hot condition and kept undisturbed at room temperature. The crystals of aluminium sulphate started to come out from solution after 10 h. This method is found to be capable of producing a considerable amount of aluminium tartrate for the study within 48 h and is regarded as an efficient route for the preparation of the present compound. Moreover, the quality of crystals obtained are highly suitable for single crystal Xrd. It is also worth mentioning that the scalability of the present compound with respect to different stoichiometry of

precursors is good. Single crystal of this compound was prepared and the cell parameters were reported [46]. We did not make single crystal Xrd studies for the compound prepared since we gave primary importance for proton conductivity of the present compound. The purity of the synthesized compound is well indicated by molecular weight determined by freezing point depression and C,H analysis, in both the measurements the obtained values are very close to theoretical values. Thus, the present method is handier than gel phase preparation method and free from gel phase impurities in addition to less duration for crystallization from solution. Hence, aluminium tartrate can be obtained directly in a single lot with the reduction of time and effort of crystallization.

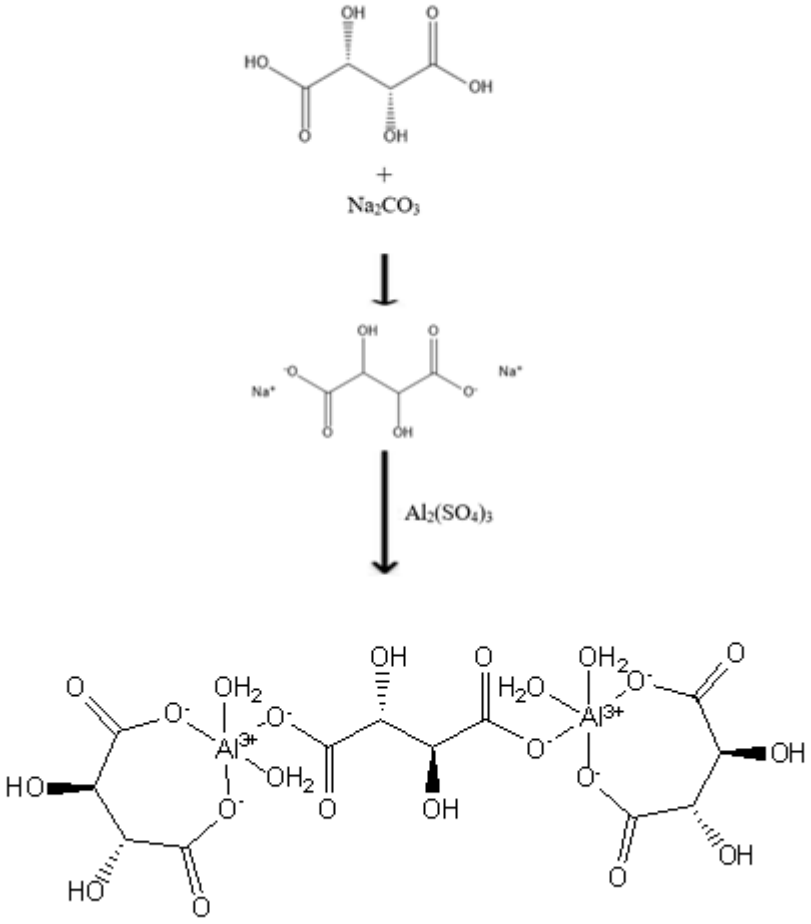


**Figure.1 Preparation of Aluminium tartrate and representation of environment around the metal ion**

The structure of aluminium tartrate can be seen in the scheme of preparation. It is clear from the structure that each $Al^{+3}$ ion is chelated by one tartrate ion and the chelated $Al^{+3}$ ions are connected by another bridging tartrate ion. The optimized three-dimensional structure of the aluminium tartrate is shown in Fig.2 and electron density of this compound in HOMO and LUMO are presented in Fig.3.

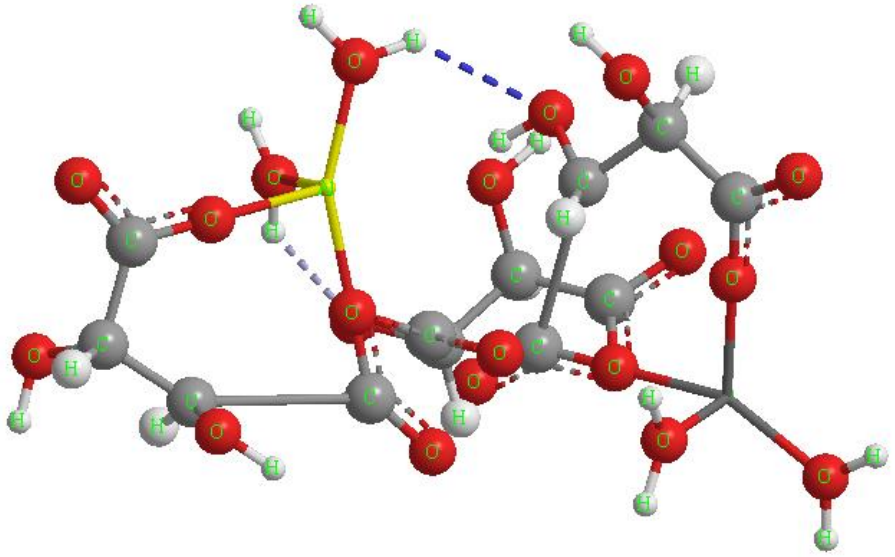

**Figure.2 Three-dimensional structure of Aluminium tartrate**

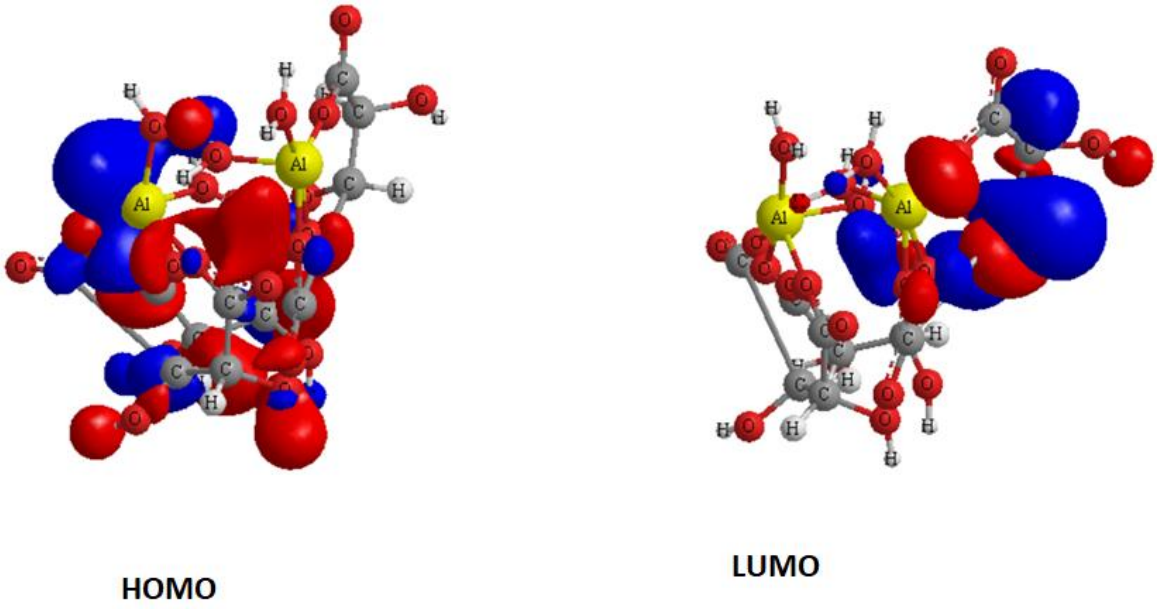


**Figure.3 The charge distribution on the HOMO and LUMO of Aluminium tartrate**

From the above structures it can be seen that the molecule has considerable electron density in the HOMO and LUMO in addition to positive charge on the metal ion. The energies of HOMO and LUMO respectively are 22.465 eV and 23.906 eV and energy gap is low, i.e. 1.441 eV, which implies the thermal energy at room temperature can promote the molecule to LUMO from HOMO. These structural features are favourable for the formation of hydrogen bonding with water molecules and are the general requirements for the humidity based proton conductivity of the compounds.

### 3.2 FTIR Analysis

The FTIR spectrum of aluminium tartrate is almost similar to most of metal tartrates reported [47-51]. The FTIR spectrum of the complex is presented in the Fig.4. The absence of characteristic peak around 1700 $cm^{-1}$ confirms the deprotonated nature of carboxylate group [50,52]. The peaks observed at 1651 $cm^{-1}$ and 1373 $cm^{-1}$ can be attributed to asymmetric and symmetric stretching of carboxylate group respectively [47-50, 52]. The difference between these peaks is ~200 $cm^{-1}$ which confirms the monodentatae nature of carboxylate group.

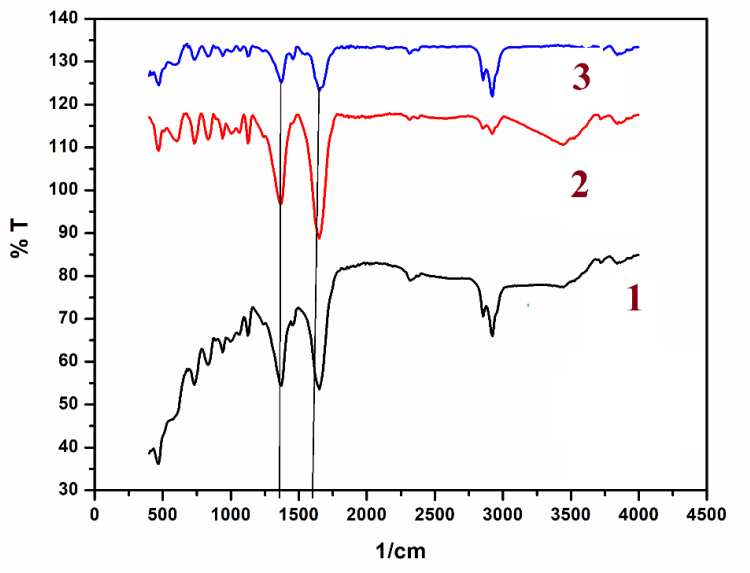


**Figure.4 FTIR spectrum of aluminium tartrate complex. (1- as synthesized, 2- after re-exposure to 100% relative humidity and 3- after exposing to 100% relative humidity for 4 h and dried in $CaCl_2$ desiccator.)**

The peaks at 1059 $cm^{-1}$ and 1126 $cm^{-1}$ indicated the C-O stretching of cis coordinated alcoholic groups[45].

The moisture dependent proton conductivity of the compound has to be analysed under varying levels of relative humidity using electrochemical impedance spectroscopy, it becomes necessary to ascertain the structural integrity of the compound under different conditions. The compound was dried under a stream of forceful warm air and re-exposed to moisture. The FTIR spectra were recorded in the dried and moisture re-exposed conditions. A perusal of Fig.4 indicates that the spectra are almost similar to FTIR spectrum of freshly prepared compound. However, a broad band around 3160 – 3590 $cm^{-1}$ is attributed to the O-H stretching of hydrogen bonded water molecules, which is absent for completely dried sample and partially observed for aluminium tartrate as synthesized [47-50]. This indicates the robustness of the compound under all chosen conditions. This is further substantiated by the PXRD characterization under different conditions of the sample, which is discussed in the following section.

### 3.3 Results of PXRD study

The structural rigidity of the compound was followed using the PXRD experiments under different humidity conditions. The PXRD of as synthesized matches well with the reported by Sato et.al [53]. This confirms the phase purity of the sample. The presence of various peaks indicates presence of well-defined different planes in the crystal as reported for the metal tartrates [54-56]. The PXRD results of synthesized sample under different humidity conditions are presented in the Fig.5.The very clear occurrences of few peaks at 20°, 37.3° and 41° can be considered for quick identification of the compound [53,54] and also implied the phase purity of the sample. The

stability of the compound upon dehydration with warm dry air and exposing to humid environment were also analysed using PXRD pattern of the compound in the corresponding environment and are also included in Fig.5

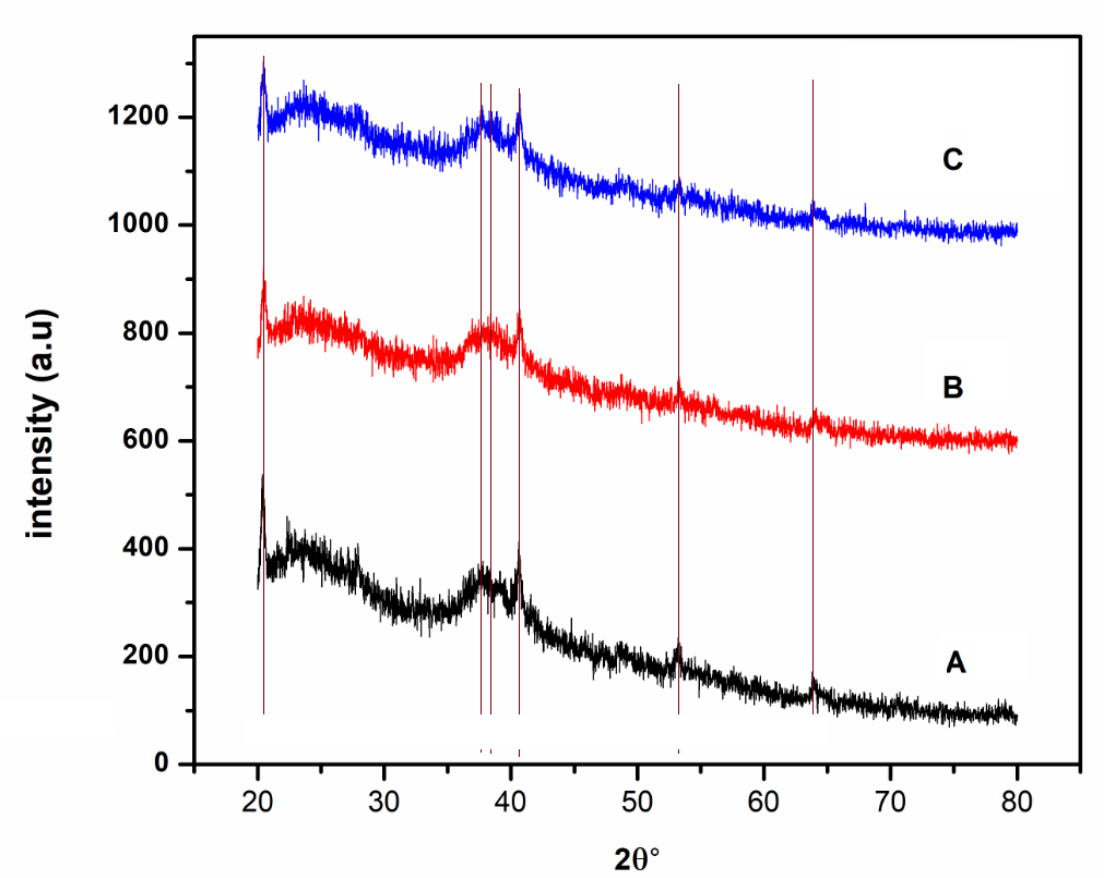


**Figure.5 The PXRD patterns of the Aluminium tartrate under different conditions. A. as synthesized B. dehydrated in warm air C. after exposing to moisture environment.**

The PXRD pattern of as synthesized sample resembles with the dehydrated sample (Fig.5B) in warm air, which indicated that the overall structural stability of the compound studied. This further supports the FTIR results of the sample under different conditions. To ascertain the stability of the compound during entry of protic vapor (water vapor), the dried powder sample was placed under 100% relative humidity environment for 24 h t 31±1°C and then PXRD pattern was recorded, which can also be seen in Fig.6. The patterns exactly match with the PXRD patterns of as synthesized and dried sample in warm air. This indicated the structural maintenance of the sample during re-entry of protic vapor. However, there are slight unnoticeable deviations in the peaks at lower angles which could be ascertained to minimal expansion of cell parameters in preferred orientations [57]. This expansion might be caused by the voluminous occlusion of the protic guest vapor. Thus, the results of FTIR and PXRD studies clearly indicated that the structural integrity of the molecule is highly maintained when protic vapor enters and leaves the molecule. The robustness of the sample is well demonstrated by FTIR and PXRD results and hence, the sample can be examined for its proton conductivity under experimental conditions given below using electrochemical impedance spectroscopy.

### 3.4 Electrochemical Impedance Analysis on proton conductivity of aluminium tartrate

Electrochemical impedance spectroscopy is the best tool for analysing the proton conductivity of solid electrolytes. In this method an AC sinusoidal voltage of a very small amplitude is superimposed on the open circuit potential at different applied frequencies and the resulting current, which is also a sinusoidal, is measured. The ratio between the applied sinusoidal voltage and resulting sinusoidal current at any applied frequency gives the impedance of the system under study at the applied frequency. The impedance is divided into real and imaginary parts and a plot between real and imaginary parts of impedance at different applied frequencies is called Nyquist or Cole-Cole plot. In the present case, the synthesized compound was pelletized and placed between two conducting metal surfaces after coating with silver paste. The current within the solid phase, placed between two conducting metal surfaces, is ionic and electrode-electrolyte interfaces are ionically blocking. Such interfaces are called ionically blocking interfaces [58]. The excess charge on one side of ionically blocking interface is balanced by excess electronic charge on the conducting metal surface [58,59].

The inherent proton conductivity of the present compound under ambient condition (around 45°C) has not reported so far. The conductivity of the material in DC range was found to be in the order $10^{-8}$ $Scm^{-1}$. This indicated very poor electronic conductance by this material and to consider the material as electronically an insulator. However, it is interesting to note that the Nyquist plots of the material changes significantly under intense humidity conditions at 30±1°C. It is also noted that the Nyquist plot is chaotic for the compound as synthesized and up to 50 minutes on exposing to 100% RH environment. After 50 minutes there's a regular shape for Nyquist plot and significant variations are observed only after 4 h in the Nyquist plots. The experimental Nyquist plots for the aluminium tartrate pellet under 100% Rh are presented in the Fig.6a, 6b and 6c.

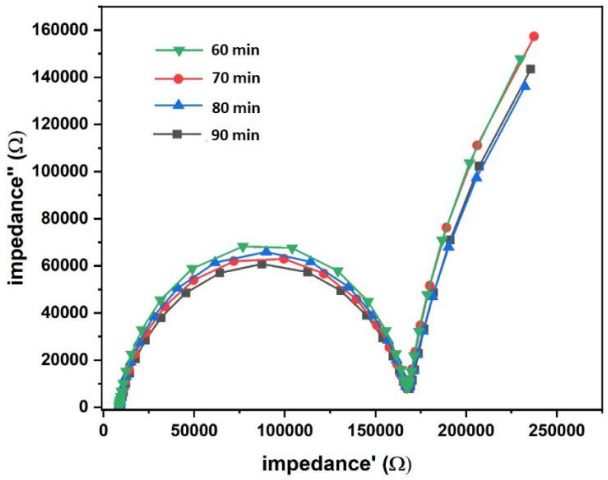


**Figure.6a Nyquist plots of the sample under 100% at 30±1°C (60-90 min)**

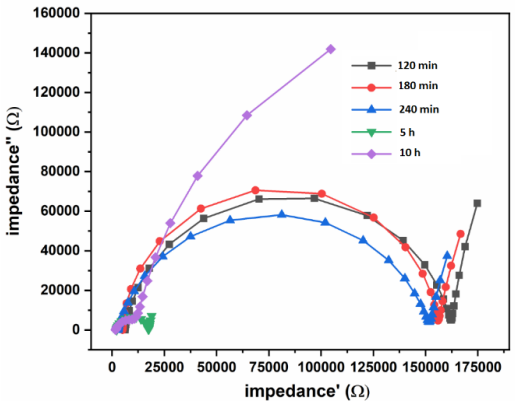


**Figure.6b Nyquist plots of the sample under 100% at 30±1°C (120 min-10 h)**

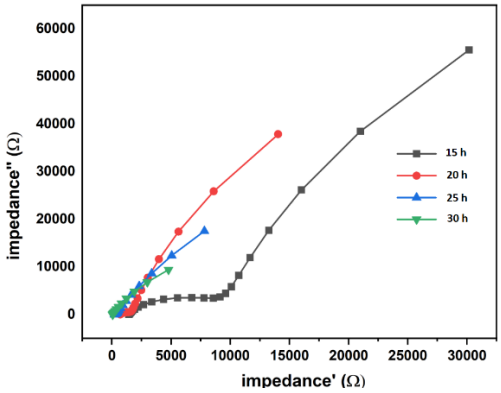


**Figure.6c Nyquist plots of the sample under 100% at 30±1°C (15 h -30 h)**

The electrochemical impedance parameters associated with the Nyquist plot can be obtained by fitting the experimental curves with a suitable equivalent circuit. In the present study the experimental curves fit well with the equivalent circuit shown in Fig.7. This equivalent circuit is one of the equivalent circuits proposed for the ionic conductance of solid-state electrolytes [58]. The Rs represents resistance offered by the electrical connections to the conducting plates. The ionic conductance of the solid electrolyte is represented in terms of charge transfer resistance Ri of the solid electrolyte [58]. The ionically conducting solid phase is in series connection with the ionically blocking electrolyte-electrode interface, hence this situation can be represented by Ri in series connection with a capacitor representing the capacitance of ionically blocking electrolyte-electrode interface [58]. However, due to surface non-uniformity i.e. surface roughness and/or accumulation of ions at the electrolyte-electrode interface, the ideal capacitance is lost and is being replaced by constant phase element (CPE) [60,61]. CPE2 represents the ionically blocking electrolyte-electrode interface. The impedance function of constant phase element is given by:

$$Z_{CPE}=\frac{1}{Y_0(j\omega)^n} \quad \text{.....(1)}$$

Where, $Y_0$ represents admittance at 1 rad $s^{-1}$ and ω is angular frequency. “n” is a constant and its value is zero for pure resistor, -1 for pure inductor and +1 for pure capacitor. In the present case the values of “n” are very close to 1 and hence the ionically blocking interface is very close to capacitor. Constant phase element1 (CPE1) represents

geometrical capacitance for the solid electrolyte between parallel plates [59]. This is normally observed at the highest frequency ranges of Nyquist plot [59]. Re is the resistance for electronic current, which is normally absent for many coordination compounds.

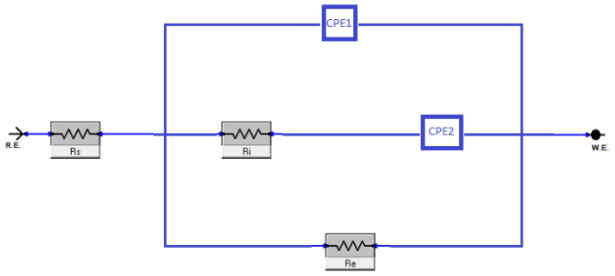


**Figure.7 Equivalent circuit fitting well with the experimental Nyquist plots**

The magnitude of AC conductivity, when the pellet is exposed to 100% RH,at 30±1°C, was found to be $2.3X10^{-4}$ $Scm^{-1}$. This value is comparable to those values reported for the metal organic frame works or coordination polymers [62-71]. Even though the protons are removed from the tartaric acid molecules before coordinating with $Al^{+3}$ ions, the origin of protonic charge in the coordination compound can be described in an analogous manner as that of ferric oxalate dihydrate system [68], which is attributed to the Lewis acidity of metal centres, that can induce the removal of proton from water molecules [27]. The proton conductivity of the sample was measured after thoroughly drying with dry air at 60°C for 4 h and then keeping in a desiccator containing anhydrous $CaCl_2$. The sample has shown very low proton conductivity of $12.4X10^{-11}$ $Scm^{-1}$, which is several orders lower than that of fully hydrated sample. This implied importance of water molecules in establishing the proton conducting network in the structure. Furthermore, the AC conductivity of the sample is several orders greater than DC conductivity, which further supports the proton conductivity of the sample rather than electronic conductivity [27,66,69].

The dried specimen after re-exposing to 100% RH at 30±1°C for 24 h, exhibited the proton conductivity $1.9X10^{-4}$ $Scm^{-1}$, this value is very close to the value obtained in the first exposure to 100% RH. This observation along with PXRD and FTIR studies demonstrated well the structural stability of the compound upon drying and exposing to moisture. Furthermore, the moisture dependent proton conductivity of the material also suggests as a promising candidate for moisture sensor. However, additional quantitative correlation between the physical conditions and structural aspects is necessary for studying moisture sensor applications and the experiments in these lines are underway in our laboratory.

The temperature dependent proton conductivity of the specimen was also studied in the temperature range 30-55°C, using electrochemical impedance spectroscopy. With increase in temperature the proton conductivity of the sample increased and this is shown in Fig.8.

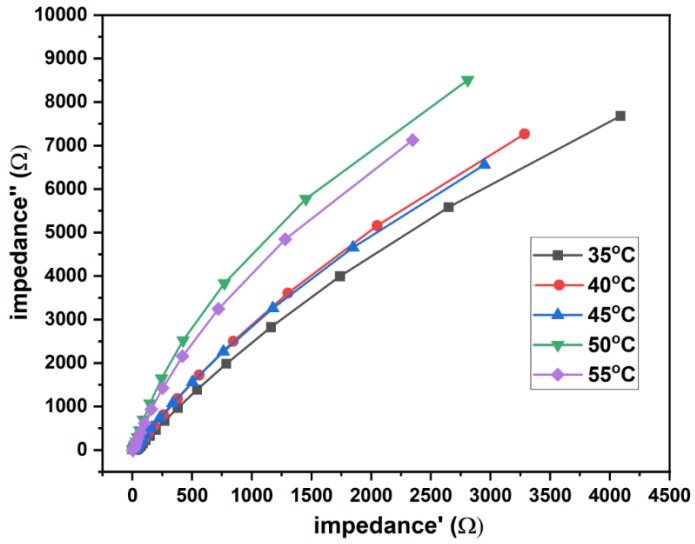


**Figure.8 Nyquist plots for the sample at various temperatures**

An Arrhenius type plot of proton conductivity at 98% RH in the above mentioned temperature range is shown in Fig.9. From this figure the activation energy was calculated for moisture dependent proton conductivity, which is $1.7X10^{-4}$ eV. This value is very low suggests Grotthuss type mechanism of proton conductivity [27] and hence the mechanism of proton conductivity can be attributed mainly on the basis of hydrogen bond reformation between $H_3O^+$ and $H_2O$ molecules involved in the complex network system.

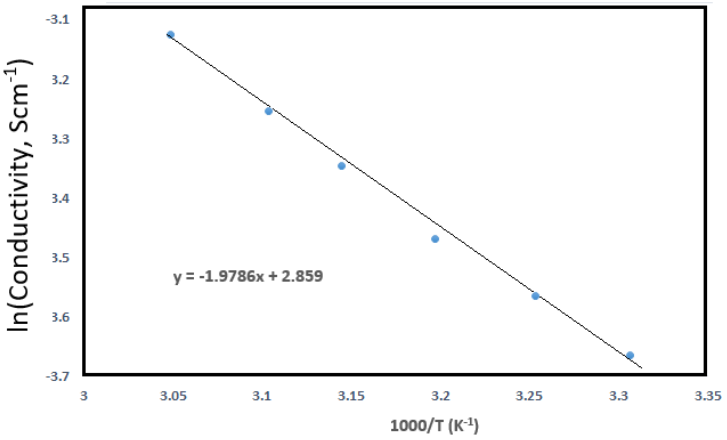


**Figure.9 Arrhenius type plot for calculation of energy of activation for proton conductivity of the sample.**

## 4. Conclusion

Aluminium(III) tartrate crystal was obtained by solution crystallization method. Its moisture dependent proton conductivity was analysed employing electrochemical impedance method. The compound exhibited good structural stability upon hydration, dehydration and rehydration. The proton conductivity of the compound depends on humidity of the environment. The proton conductivity of the compound increased with time on exposing to moist environment and is reversible. The effect of temperature on proton conductivity of the sample implied the Grotthuss type proton conductivity.

## REFERENCES


[1] Ratnamala A, Rao VK, Raja KP. Metal-organic framework membranes for proton exchange membrane fuel cells: A mini-review. Inorganica Chimica Acta. 2022 Nov 24:121304.

[2] Ren HM, Liu BY, Zuo BT, Li ZF, Li G. The effect of free carboxylic acid groups on the proton conductivity of a series of UiO-66-Ce (IV) metal-organic frameworks. Microporous and Mesoporous Materials. 2023 Mar 1;351:112481.

[3] Sharma A, Lim J, Lah MS. Strategies for designing metal–organic frameworks with superprotonic conductivity. Coordination Chemistry Reviews. 2023 Mar 15;479:214995.

[4] Goldemberg J. Ethanol for a sustainable energy future. science. 2007 Feb 9;315(5813):808-10.

[5] Zhang Z, Yao ZZ, Xiang S, Chen B. Perspective of microporous metal–organic frameworks for CO 2 capture and separation. Energy & environmental science. 2014;7(9):2868-99.

[6] Zhu L, Zhu H, Wang L, Lei J, Liu J. Efficient proton conduction in porous and crystalline covalent-organic frameworks (COFs). Journal of Energy Chemistry. 2023 Apr 14.

[7] Zhang Q, Dong S, Shao P, Zhu Y, Mu Z, Sheng D, Zhang T, Jiang X, Shao R, Ren Z, Xie J. Covalent organic framework–based porous ionomers for high-performance fuel cells. Science. 2022 Oct 14;378(6616):181-6.

[8] Jiao K, Xuan J, Du Q, Bao Z, Xie B, Wang B, Zhao Y, Fan L, Wang H, Hou Z, Huo S. Designing the next generation of proton-exchange membrane fuel cells. Nature. 2021 Jul 15;595(7867):361-9.

[9] Moghaddam S, Pengwang E, Jiang YB, Garcia AR, Burnett DJ, Brinker CJ, Masel RI, Shannon MA. An inorganic–organic proton exchange membrane for fuel cells with a controlled nanoscale pore structure. Nature Nanotechnology. 2010 Mar;5(3):230-6.

[10] Trigg EB, Gaines TW, Maréchal M, Moed DE, Rannou P, Wagener KB, Stevens MJ, Winey KI. Self-assembled highly ordered acid layers in precisely sulfonated polyethylene produce efficient proton transport. Nature materials. 2018 Aug;17(8):725-31.

[11] Zhao X, Meng X, Zou H, Zhang Y, Ma Y, Du Y, Shao Y, Qi J, Qiu J. Nano-enabled solar driven-interfacial evaporation: Advanced design and opportunities. Nano Research. 2023 May;16(5):6015-38.

[12] Zhang H, Shen PK. Advances in the high performance polymer electrolyte membranes for fuel cells. Chemical Society Reviews. 2012;41(6):2382-94.

[13] Hickner MA, Ghassemi H, Kim YS, Einsla BR, McGrath JE. Alternative polymer systems for proton exchange membranes (PEMs). Chemical reviews. 2004 Oct 13;104(10):4587-612.

[14] Wachsman ED, Lee KT. Lowering the temperature of solid oxide fuel cells. Science. 2011 Nov 18;334(6058):935-9.

[15] Zhang H, Shen PK. Recent development of polymer electrolyte membranes for fuel cells. Chemical reviews. 2012 May 9;112(5):2780-832.

[16] Wu S, Liu Y, Wang C, Dai H, Wang X, Bi L. Cobalt-free LaNi0. 4Zn0. 1Fe0. 5O3-δ as a cathode for solid oxide fuel cells using proton-conducting electrolyte. International Journal of Hydrogen Energy. 2021 Nov 8;46(77):38482-9.

[17] Chen YY, Wang ZY, Liu YR, Zhang X. Solvent-induced high proton conductivity of a water-stable three-dimensional Mn (II) metal-organic framework. Journal of Solid State Chemistry. 2023 Sep 25:124354.

[18] Liu L, Li X, Liu Z, Zhang S, Qian L, Chen Z, Li J, Fang P, He C. High-performance fuel cells using Nafion composite membranes with alignment of sulfonated graphene oxides induced by a strong magnetic field. Journal of Membrane Science. 2022 Jul 5;653:120516.

[19] Thuc VD, Tinh VD, Kim D. Simultaneous improvement of proton conductivity and chemical stability of Nafion membranes via embedment of surface-modified ceria nanoparticles in membrane surface. Journal of Membrane Science. 2022 Feb 15;642:119990.

[20] Long J, Zhang X, Zeng S, Pei T, Ma H, Li X, Meng X. Constructing a long-range proton conduction bridge in sulfonated polyetheretherketone membranes with low DS by incorporating acid-base bi-functionalized metal organic frameworks. International Journal of Hydrogen Energy. 2023 Jan 15;48(5):2001-12.
[21] Karimi MB, Mohammadi F, Hooshyari K. Recent approaches to improve Nafion performance for fuel cell applications: A review. International Journal of Hydrogen Energy. 2019 Nov 5;44(54):28919-38.
[22] Hsu WY, Gierke TD. Ion transport and clustering in Nafion perfluorinated membranes. Journal of Membrane Science. 1983 Feb 1;13(3):307-26.
[23] Kanda S, Yamashita K, Ohkawa K. A proton conductive coordination polymer. I.[N, N′-bis (2-hydroxyethyl) dithiooxamido] copper (II). Bulletin of the Chemical Society of Japan. 1979 Nov;52(11):3296-301.
[24] Ghanbari T, Abnisa F, Daud WM. A review on production of metal organic frameworks (MOF) for CO2 adsorption. Science of The Total Environment. 2020 Mar 10;707:135090.
[25] Abuzalat O, Tantawy H, Baraka A. Advanced oxidation process using cobalt-based metal-organic frameworks via operating Co (II)/Co (III) redox cycling for efficient organic contaminant degradations. Journal of Water Process Engineering. 2023 Aug 1;54:103938.
[26] Kitagawa H. Transported into fuel cells. Nature chemistry. 2009 Dec;1(9):689-90.
[27] Saravanabharathi D, Obulichetty M, Rameshkumar S, Kumaravel M. Rapid crystallization and proton conductivity of copper (II)-l-tartrate. Synthetic metals. 2012 Oct 1;162(17-18):1519-23.
[28] Liu YR, Chen YY, Zhuang Q, Li G. Recent advances in MOFs-based proton exchange membranes. Coordination Chemistry Reviews. 2022 Nov 15;471:214740.
[29] Jagur-Grodzinski J. Polymeric materials for fuel cells: concise review of recent studies. Polymers for Advanced Technologies. 2007 Oct;18(10):785-99.
[30] Chen Z, Lu C. Humidity sensors: a review of materials and mechanisms. Sensor letters. 2005 Dec 1;3(4):274-95.
[31] Phair JW, Badwal SP. Review of proton conductors for hydrogen separation. Ionics. 2006 Jul;12(2):103-15.
[32] Lee HY. A Study on the Synthesis of Aluminum Tartrate from Aluminum Chloride Solutions. Resources Recycling. 2011;20(2):54-9.
[33] Ramaswamy P, Wong NE, Shimizu GK. MOFs as proton conductors–challenges and opportunities. Chemical Society Reviews. 2014;43(16):5913-32.
[34] Horike S, Umeyama D, Kitagawa S. Ion conductivity and transport by porous coordination polymers and metal–organic frameworks. Accounts of chemical research. 2013 Nov 19;46(11):2376-84.
[35] Shimizu GK, Taylor JM, Kim S. Proton conduction with metal-organic frameworks. Science. 2013 Jul 26;341(6144):354-5.
[36] Yoon M, Suh K, Natarajan S, Kim K. Proton conduction in metal–organic frameworks and related modularly built porous solids. Angewandte Chemie International Edition. 2013 Mar 4;52(10):2688-700.
[37] Kitagawa H. Transported into fuel cells. Nature chemistry. 2009 Dec;1(9):689-90.
[38] Hawthorne FC, Borys I, Ferguson RB. Structure of calcium tartrate tetrahydrate. Acta Crystallographica Section B: Structural Crystallography and Crystal Chemistry. 1982 Sep 15;38(9):2461-3.
[39] Shajan XS, Mahadevan C. On the growth of calcium tartrate tetrahydrate single crystals. Bulletin of Materials Science. 2004 Aug;27:327-31.
[40] Suthar SR, Joshi MJ. Growth and characterization of Mn2+ doped calcium l-tartrate crystals. Crystal Research and Technology: Journal of Experimental and Industrial Crystallography. 2006 Jul;41(7):664-70.
[41] Selvarajan P, Das BN, Gon HB, Rao KV. Infrared spectroscopic and thermal studies of calcium tartrate single crystals grown by silica-gel technique. Journal of materials science letters. 1993 Jan;12:1210-1.
[42] Torres ME, Peraza J, Yanes AC, López T, Stockel J, Marrero-Lopez D, Solans X, Bocanegra E, Silgo CG. Electrical conductivity of doped and undoped calcium tartrate. Journal of Physics and Chemistry of Solids. 2002 Apr 1;63(4):695-8.

[43] Mathivanan V, Haris M, Chandrasekaran J. Experimental investigation of the structure, magnetic moment and decomposition process on heating in dipotassium tartarte crystals grown in chemical reaction gel method. Optik. 2016 May 1;127(9):3892-5.
[44] Patel AR, Venkateswara Rao A. Crystal growth in gel media. Bulletin of Materials Science. 1982 Dec;4:527-48.
[45] Saravanabharathi D, Obulichetty M, Rameshkumar S, Kumaravel M. Humidity based proton conductivity of calcium-l-tartrate tetrahydrate: An environmentally benign coordination polymer as a solid electrolyte. Synthetic metals. 2014 Oct 1;196:76-82.
[46] Lee HY. A Study on the Synthesis of Aluminum Tartrate from Aluminum Chloride Solutions. Resources Recycling. 2011;20(2):54-9.
[47] Kotru PN, Raina KK, Koul ML. Characterization of lanthanum heptamolybdate crystals grown from silica gel. Journal of Materials Science. 1986;21:3933-40.
[48] Dass N, Sarmah S. Synthesis and Thermal Decomposition of [Ni 2 (C 4 H 4 O 6) 2]· 7H 2 O. Journal of thermal analysis and calorimetry. 1999 Oct 25;58(1):137-45.
[49] Du YE, Han ZB. Hydrothermal synthesis and structural characterization of a new 3D chiral coordination polymer [Cd 2 (C 4 H 4 O 6) 2] n. Russian Journal of Coordination Chemistry. 2011 Jul;37:506-10.
[50] Rodrigues EC, Carvalho CT, de Siqueira AB, Bannach G, Ionashiro M. Synthesis, characterization and thermal behaviour on solid tartrates of some bivalent metal ions. Thermochimica acta. 2009 Dec 10;496(1-2):156-60.
[51] Joshi SJ, Parekh BB, Vohra KD, Joshi MJ. Growth and characterization of gel grown pure and mixed iron-manganese levo-tartrate crystals. Bulletin of Materials Science. 2006 Jun;29:307-12.
[52] Saravanabharathi D, Obulichetty M, Rameshkumar S, Kumaravel M. Rapid crystallization and proton conductivity of copper (II)-l-tartrate. Synthetic metals. 2012 Oct 1;162(17-18):1519-23.
[53] Sato T, Ikoma S, Ozawa F. Thermal decomposition of aluminium hydroxycarboxylates—lactate, citrate and tartrate. Journal of Chemical Technology and Biotechnology. Chemical Technology. 1983 Nov;33(8):415-20.
[54] Mathivanan V, Haris M, Prasanyaa T, Amgalan M. Synthesis and characterization of gel-grown cobalt tartrate crystals. Pramana. 2014 Mar;82:537-48.
[55] Rethinam FJ, Oli DA, Ramasamy S, Ramasamy P. Growth and Characterisation of Pure and Nickel-doped Strontium Tartrate Tetrahydrate Single Crystals. Crystal Research and Technology. 1993;28(6):861-5.
[56] Reema KB, Jagannatha N. Thermal and optoelectrical properties of cobalt doped and undoped strontium L (+) tartrate pentahydrate single crystals. Materials Today: Proceedings. 2022 Jan 1;49:1323-30.
[57] Fridriksson T, Bish DL, Bird DK. Hydrogen-bonded water in laumontite I: X-ray powder diffraction study of water site occupancy and structural changes in laumontite during room-temperature isothermal hydration/dehydration. American Mineralogist. 2003 Feb 1;88(2-3):277-87.
[58] Raleigh DO. Electrode Processes in Solid-Electrolyte Systems.
[59] Huggins RA. Simple method to determine electronic and ionic components of the conductivity in mixed conductors a review. Ionics. 2002 May;8:300-13.
[60] Mallaiya K, Subramaniam R, Srikandan SS, Gowri S, Rajasekaran N, Selvaraj A. Electrochemical characterization of the protective film formed by the unsymmetrical Schiff's base on the mild steel surface in acid media. Electrochimica Acta. 2011 Apr 15;56(11):3857-63.
[61] Danaee I, RameshKumar S, RashvandAvei M, Vijayan M. Electrochemical and quantum chemical studies on corrosion inhibition performance of 2, 2'-(2-hydroxyethylimino) bis [N-(alphaalpha-dimethylphenethyl)-N-methylacetamide] on mild steel corrosion in 1M HCl solution. Materials Research. 2020 Jun 1;23.
[62] Nagao Y, Fujishima M, Ikeda R, Kanda S, Kitagawa H. Highly proton-conductive copper coordination polymers. Synthetic metals. 2003 Mar 13;133:431-2.

[63] Nagao Y, Ikeda R, Iijima K, Kubo T, Nakasuji K, Kitagawa H. A new proton-conductive copper coordination polymer,(HOC3H6) 2dtoaCu (dtoa= dithiooxamide). Synthetic metals. 2003;135:283-4.
[64] Nagao Y, Kubo T, Nakasuji K, Ikeda R, Kojima T, Kitagawa H. Preparation and proton transport property of N, N′-diethyldithiooxamidatocopper coordination polymer. Synthetic metals. 2005 Sep 22;154(1-3):89-92.
[65] Kitagawa H, Nagao Y, Fujishima M, Ikeda R, Kanda S. Highly proton-conductive copper coordination polymer, H2dtoaCu (H2dtoa= dithiooxamide anion). Inorganic Chemistry Communications. 2003 Mar 1;6(4):346-8.
[66] Nagao Y, Kubo T, Nakasuji K. Synthetic Met. 2005, 154, 89–92; b) H. Kitagawa, Y. Nagao, M. Fujishima, R. Ikeda, S. Kanda. Inorg. Chem. Commun. 2003;6:346-8.
[67] Sadakiyo M, Yamada T, Kitagawa H. Rational designs for highly proton-conductive metal− organic frameworks. Journal of the American Chemical Society. 2009 Jul 29;131(29):9906-7.
[68] Yamada T, Sadakiyo M, Kitagawa H. High proton conductivity of one-dimensional ferrous oxalate dihydrate. Journal of the American Chemical Society. 2009 Mar 11;131(9):3144-5.
[69] Xie L, Lin J, Liu X, Xue W, Zhang W, Liu S, Zhang J, Chen X. Organic ammonium ion-occluded flexible coordination polymers: Thermal activation, structure transformation and proton transfer. Science China Chemistry. 2010 Oct;53:2144-51.
[70] Dey C, Kundu T, Banerjee R. Reversible phase transformation in proton conducting Strandberg-type POM based metal organic material. Chemical communications. 2012;48(2):266-8.
[71] Sahoo SC, Kundu T, Banerjee R. Helical water chain mediated proton conductivity in homochiral metal–organic frameworks with unprecedented zeolitic unh-topology. Journal of the American Chemical Society. 2011 Nov 9;133(44):17950-8.

DOI: https://doi.org/10.15379/ijmst.v10i2.3042